Solar Energy 178 (2019) 331–340

Contents lists available at ScienceDirect

Solar Energy

journal homepage: www.elsevier.com/locate/solener

# Design and operating considerations for a shell-and-plate, moving packed-bed, particle-to-$sCO_2$ heat exchanger

Kevin J. Albrecht*, Clifford K. Ho

*Concentrating Solar Technologies Department, Sandia National Laboratories, 1515 Eubank Blvd. SE, Albuquerque, NM 87123, USA*

ARTICLE INFO

*Keywords:*
Heat exchanger
Particle
Supercritical
Carbon dioxide

ABSTRACT

An efficient modeling methodology for simulating moving packed-bed heat exchangers for the application of particle-to-$sCO_2$ heat transfer in next-generation concentrating solar power (CSP) plants is presented. Moving packed-bed heat exchangers have application to power-cycle heat addition for particle-based CSP plants and indirect energy storage for direct $sCO_2$ CSP receivers. Further development of moving packed-bed heat exchangers for application to commercial CSP systems requires numerical simulation tools for the design and evaluation of particle-to-$sCO_2$ heat transfer. In this paper, a steady-state reduced-order model of a shell-and-plate moving packed-bed heat exchanger is presented and used to investigate design considerations and performance limitations. The model appropriately captures the flow configuration of a multi-bank shell-and-plate design where the local cross-flow and global counter-flow configurations are addressed. This allows for the design tradeoffs in heat exchanger geometry and particle properties to be explored on the heat exchanger conductance and $sCO_2$ pressure drop. Overall heat transfer coefficients for the particle-to-$sCO_2$ heat exchanger at CSP operating temperature (500–800 °C) can approach 400 $W\,m^{-2}\,K^{-1}$ using particle channel dimensions of 4 mm with particle diameters of 200 μm. The sensitivity of particle thermophysical properties was also explored to identify important parameters for improving the overall heat transfer coefficient that can be leveraged in the development of alternative particles. Packed bed void fraction and solid thermal conductivity were identified to be areas for potential improvement of sintered bauxite particles, which could increase the overall heat transfer coefficient by up to 60 $W\,m^{-2}\,K^{-1}$. To achieve DOE cost targets (< \$150 $kW_t^{-1}$) for $sCO_2$ power cycle heat addition, diffusion bonded plates containing $sCO_2$ microchannels must be produced at less than \$2400 $m^{-2}$ for the moving packed-bed heat exchanger to become commercially viable.

## 1. Introduction

Particle-based CSP concepts continue to receive high levels of attention as a potential path toward increasing the operating temperature of CSP plants (Ho, 2016; Ma et al., 2015). The key advantage of high-temperature operation is the ability to drive high-efficiency power cycles such as $sCO_2$ or air Brayton (Stein & Buck, 2017; Turchi et al., 2013; Carlson et al., 2017). In addition to the concept of particles as a receiver heat transfer fluid, particles have also been proposed as an indirect thermal energy storage media for volumetric or direct $sCO_2$ receivers (Zanganeh et al., 2012; Alvia-Marin, 2011). However, heat exchangers for the indirect transfer of thermal energy between high-temperature (> 700 °C) particles and high-pressure (> 20 MPa) $sCO_2$ have yet to achieve cost targets.

The majority of the work to date on particle-based CSP concepts has focused on receiver development since the solar-to-electric efficiency of a CSP plant is directly linked to the receiver thermal efficiency and operating temperature. Thus, it is imperative that the efficiency of the solar thermal receiver approach the blackbody limit for achieving cost targets. The maximum solar-to-electric efficiency is given by the following expression, which is the product of the Carnot efficiency for the power cycle and the maximum blackbody efficiency of the receiver.

$$\eta = \underbrace{\left(1 - \frac{T_L}{T_H}\right)}_{\text{Carnot Efficiency}} \underbrace{\left(1 - \frac{\sigma (T_H + \Delta T_{HX})^4}{C\, q_{DNI}}\right)}_{\text{Receiver Efficiency}} \quad (1)$$

However, the operating temperature of the receiver is influenced by the power-cycle heat addition temperature ($T_H$) and particle-to-$sCO_2$ temperature drop across the power-cycle primary heat exchanger ($\Delta T_{HX}$). Without effective particle-to-$sCO_2$ heat transfer, the temperature drop across the heat exchanger could reduce solar-to-electric efficiency just the same as an inefficient solar thermal receiver. For every

* Corresponding author.
*E-mail address:* kalbrec@sandia.gov (K.J. Albrecht).

https://doi.org/10.1016/j.solener.2018.11.065
Received 18 September 2018; Received in revised form 15 November 2018; Accepted 28 November 2018
Available online 27 December 2018
0038-092X/ 

**Nomenclature**

| | |
|---|---|
| $A_{HX}$ | heat transfer area ($m^2$) |
| $C$ | concentration ratio |
| $C_A$ | cost per area ($\$\ m^{-2}$) |
| $\dot{C}_{max}$ | maximum thermal capacitance ($W\,K^{-1}$) |
| $\dot{C}_{min}$ | minimum thermal capacitance ($W\,K^{-1}$) |
| $C_P$ | cost per power ($\$\ W^{-1}$) |
| $c_{p,s}$ | solid particle specific heat capacity ($J\,kg^{-1}\,K^{-1}$) |
| $C_R$ | capacitance ratio |
| $D_h$ | hydraulic diameter (m) |
| $d_p$ | particle diameter (m) |
| Gz | Graetz number |
| $H$ | plate height (particle flow direction) (m) |
| $h_{CO_2}$ | $CO_2$ enthalpy ($J\,kg^{-1}$) |
| $\bar{h}_{CO_2}$ | $CO_2$ convection coefficient ($W\,m^{-2}\,K^{-1}$) |
| $h_s$ | solid enthalpy ($J\,kg^{-1}$) |
| $\bar{h}_{sw}$ | solid-wall convection coefficient ($W\,m^{-2}\,K^{-1}$) |
| $k_g$ | gas phase thermal conductivity ($W\,m^{-1}K^{-1}$) |
| $k_m$ | heat exchanger material thermal conductivity ($W\,m^{-1}K^{-1}$) |
| $k_s$ | particle material thermal conductivity ($W\,m^{-1}K^{-1}$) |
| $k_{s,eff}$ | bulk effective thermal conductivity of the solid particles ($W\,m^{-1}K^{-1}$) |
| $L$ | plate width ($sCO_2$ flow direction) (m) |
| $\dot{m}_{CO_2}$ | $CO_2$ mass flow rate ($kg\,s^{-1}$) |
| $\dot{m}_s$ | solid mass flow rate ($kg\,s^{-1}$) |
| NTU | number of transfer units |
| $\bar{Nu}_{D_h}$ | average Nusselt number |
| $P$ | pressure (Pa) |
| | Peclet number based on hydraulic diameter |
| $q_{DNI}$ | direct normal insolation ($W\,m^{-2}$) |
| $\dot{Q}_{HX}$ | heat exchanger thermal duty (W) |
| $R_c''$ | near-wall thermal resistance ($m^2K\,W^{-1}$) |
| $T_{CO_2}$ | $CO_2$ temperature (K) |
| $T_H$ | carnot cycle high-temperature heat addition (K) |
| $T_L$ | carnot cycle low-temperature heat rejection (K) |
| $t_m$ | heat exchanger material thickness (m) |
| $T_s$ | solid particle temperature (K) |
| $U_{HX}$ | overall heat transfer coefficient ($W\,m^{-2}\,K^{-1}$) |
| $w_{ch}$ | particle channel width (m) |

*Greek*

| | |
|---|---|
| $\alpha$ | thermal diffusivity ($m^2\,s^{-1}$) |
| $\Delta T_{HX}$ | heat exchanger temperature drop (K) |
| $\Delta T_{lm}$ | log mean temperature difference (K) |
| $\Delta P_{CO_2}$ | $CO_2$ pressure drop (Pa) |
| $\varepsilon_{HX}$ | heat exchanger effectiveness |
| $\varepsilon_s$ | solid particle emissivity |
| $\eta$ | efficiency |
| $\rho_s$ | solid particle density ($kg\,m^{-3}$) |
| $\sigma$ | Stefan-Boltzmann constant ($W\,m^{-2}\,K^{-4}$) |
| $\phi$ | particle contact term |
| $\phi_g$ | gas volume fraction of packed bed |
| $\phi_s$ | solid volume fraction of packed bed |

additional 10 °C temperature drop across the heat exchanger, the solar-to-electric efficiency is reduced by 0.5%. Therefore, the power cycle heat addition heat exchanger must be developed and tested alongside the solar thermal receiver for the realization of solid particle heat transfer media.

For particle-based CSP plants, fluidized-bed heat transfer is an attractive option for primary power cycle heat addition due to the mature nature of the technology (Gomez-Garcia et al., 2017; Ma & Martinek, 2017). However, fluidization gas requirements and operational complexity have led to concerns with their ability to achieve CSP cost targets (Ho et al., 2018). Moving packed-bed heat exchangers (Fig. 1) have emerged as a simple and cost-effective alternative to fluidized-bed heat exchangers (Albrecht & Ho, 2017, 2018; Baumann & Zunft, 2015a; Baumann & Zunft, 2012) for the application of CSP power cycle heat addition. Baumann and Zunft (Baumann & Zunft, 2015a; Baumann & Zunft, 2012) developed a moving packed-bed heat exchanger, which uses horizontal tubes to contain the working fluid with a high-temperature cascading granular flow. The heat exchanger was tested at 400 °C and used thermal oil as the low-temperature fluid. Heat transfer coefficients of 200 $W\,m^{-2}\,K^{-1}$ were demonstrated with heat exchanger effectiveness of approximately 90%.

In this paper, the design considerations for a moving packed-bed

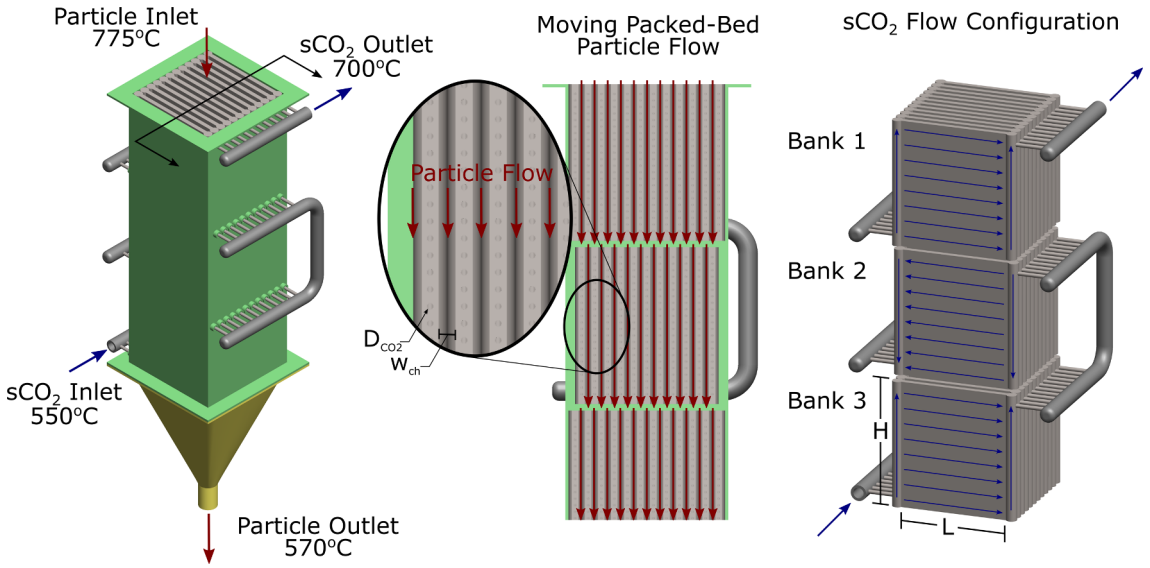


**Fig. 1.** Illustration of a particle-to-$sCO_2$ moving packed-bed heat exchanger geometry for the application of power cycle heat addition. Blue arrows represent the $sCO_2$ flow configuration and the red arrows represent the particle flow (Albrecht & Ho, 2018).

shell-and-plate heat exchanger for heating or cooling high-pressure $sCO_2$ are discussed through the development and utilization of reduced-order modeling tools.

## 2. Principles of moving packed-bed heat transfer

An illustration of a shell-and-plate moving packed-bed heat exchanger geometry is provided in Fig. 1. The geometry is shown to contain several banks of parallel plates in a vertical orientation. Globally, the heat exchanger is in a counter-flow configuration where $sCO_2$ flows in a serpentine fashion through the parallel plates from the base to the top of the heat exchanger. However, the flow configuration within individual banks of plates is in cross-flow configuration where the $sCO_2$ flow in the heat transfer region is horizontal and the particle flow is in the vertical direction. The particle flow moves downward in between the parallel plates under the force of gravity in a dense granular regime. Since the flow is controlled from the bottom up, the particles remain at or near their packing limit throughout the volume of the heat exchanger. The dense granular flow provides good contact between the particles and the heat transfer surface, which will be shown to be imperative to the heat transfer performance. The heat transfer from the high-temperature particles to the $sCO_2$ contained in the parallel plates is limited by the relatively low thermal conductivity of the particle bed ($0.2–0.6\,W\,m^{-1}K^{-1}$) (Godbee & Ziegler, 1966; Baumann & Zunft, 2015b).

Moving packed-bed heat transfer is fundamentally different from fluidized bed heat transfer, which promotes particle mixing through the use of a fluidization gas. Intermittently disrupting a packed bed of particles with a fluidization gas enhances the heat transfer coefficient by rapidly refreshing particles that cool at the heat transfer surface with high-temperature particles from the bulk flow, which results in a thin thermal boundary layer (i.e., short heat diffusion length). Although particle mixing promotes heat transfer, the heat ultimately flows through the dense particle phase when it is in direct contact with the heat transfer surface (Chen et al., 2005).

In contrast to a fluidized bed refreshing particles at a heat transfer surface, a thin thermal boundary layer can be maintained in a moving packed-bed heat exchanger through dense granular flows in narrow vertical channels, which avoids the need for a fluidization gas. Similar to microchannel heat exchangers, this approach exploits the geometric heat transfer enhancement of narrow channels, but for the physics of particle flows. In addition, the particles are always in contact with the heat transfer surface, which is an advantage over fluidized beds that have reduced particle contact times (Chen et al., 2005). Therefore, it is possible to attain heat transfer coefficients in moving packed-bed heat exchangers that approach the values ($> 500\,W\,m^{-2}K^{-1}$) that are typically associated with fluidized bed technology (Watkins & Gould, 2017).

The challenge in achieving such heat transfer coefficients is in the realization of a parallel plate design. With parallel plates, achieving true counter-flow operation is difficult, which is the reason multiple cross-flow banks (Fig. 1) are used to approximate counter-flow operation. In addition, achieving a uniform and consistent flow of particles between the parallel channels is a challenge, especially at CSP operating temperatures (Albrecht & Ho, 2018). Thus, channel widths must be constrained by particle size and particle-wall friction at operating temperature. The manufacture of the plates is another challenge, which must utilize printed circuit heat exchanger (PCHE) technology to accommodate the high-pressure $sCO_2$. To address these challenges and identify the most important design parameters for achieving high heat exchanger conductance, reduced order numerical modeling tools, which capture all the relevant physics, must be developed. Detailed design studies for prototype construction should leverage CFD design tools that can resolve 3-D temperature profiles and address thermo-mechanical stress considerations. However, the model developed here can be used to guide the heat exchanger design and choice of granular material.

## 3. Prior work in moving packed-bed heat transfer

Moving packed-bed heat transfer has been investigated in the literature, but mostly for applications other than CSP. However, the fundamental learnings of the studies provide experience on the operation of a moving packed-bed heat exchanger for the application of particle-to-$sCO_2$ heat transfer. A complete review of relevant moving packed-bed experimental and modeling work was provided in Albrecht & Ho (2017) and is summarized here highlighting the most relevant work.

The majority of moving-packed bed heat exchanger work has been directed at tubes in either a vertical (Henda & Falcioni, 2006; Park, 1996; Obuskovic, 1988) or horizontal (Baumann & Zunft, 2015a; Niegsch et al., 1994; Hiromi, 1996; Obuskovic, 1985) configuration. Concepts of using staggered horizontal tube arrays have been proposed for disrupting the thermal boundary layer that forms around a single tube such that the flow is always in the thermally developing regime. However, the heat transfer coefficient at the top and bottom surfaces of horizontal tubes have been observed to be significantly decreased due to stagnation and void regions (Niegsch et al., 1994). Therefore, the side surfaces of horizontal tubes are the most effective surfaces for moving packed-bed heat transfer.

To overcome the limitations of horizontal tube arrays and take advantage of vertically oriented heat transfer surfaces, vertical tubes or parallel plates have been proposed. Vertically oriented heat transfer surfaces allow for uniform and consistent particle flows and short heat diffusion lengths. The hydrodynamics of moving packed beds in vertical channels have been investigated through flow visualization (Obuskovic, 1988). The particles have been reported to move at a constant velocity that is well represented by a zero-shear stress boundary condition or plug flow. Nusselt numbers for the flows in ideal geometries can be determined through analytical solutions of the advection diffusion equation with a uniform velocity field. The local and average Nusselt numbers for parallel plates with constant heat flux and temperature boundary conditions are plotted in Fig. 2. For thermally developed flow, the Nusselt number asymptotes to values of 12 and 9.87 for constant heat flux and temperature boundary conditions, respectively (Albrecht & Ho, 2017; Muzychka et al., 2010). The non-dimensional length that characterizes the point at which the flow becomes thermally developed is the inverse Graetz number ($Gz^{-1} = L/Pe_{D_h}D_h$), which depends on the channel geometry and ratio of advection to conduction as characterized by the Peclet number ($Pe_{D_h} = v\,D_h/\alpha$). An enhanced local heat transfer coefficient can be observed for inverse Graetz numbers less than 0.05. Thus, designing a heat exchanger that can exploit the

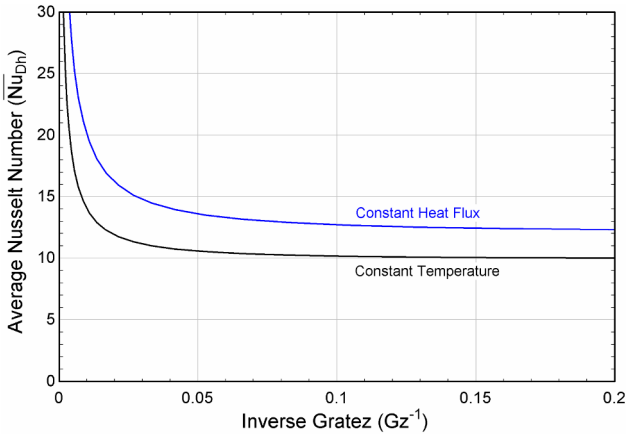


**Fig. 2.** Non-dimensional heat transfer coefficients ($\overline{Nu}_{Dh}$) for plug flow between parallel plates as a function of non-dimensional length ($Gz^{-1}$) for constant temperature and heat flux boundary conditions.

thermally developing region will be able to achieve higher overall heat transfer coefficients.

In order to disrupt the thermal boundary layer that develops in the vertical channels of a parallel plate heat exchanger, staggering banks of plates (Fig. 1) has been proposed (Byman et al., 2014). Ideally, the flow would always be kept in the thermally developing regime. However, transitioning between plate banks requires headers to accommodate the $sCO_2$ flow between plates. In addition, the cross-sectional flow area for $sCO_2$ is reduced with increasing number of banks, which directly results in increased pressure drop of the $sCO_2$ across the heat exchanger.

To better understand the engineering tradeoffs when specifying the geometry and operating conditions of a shell-and-plate moving packed-bed heat exchanger, it is necessary to develop robust and light weight modeling tools.

## 4. Particle-to-$sCO_2$ heat exchanger model

The approach of modeling moving packed beds of particles as a single component continuum has been well established in the literature (Park, 1996; Henda & Falcioni, 2006). This approach considers the multiphase particle-gas flow to be represented by a single component with thermodynamic and transport properties that appropriately characterize the mixture, which is to say that a single set of conservation equations can represent the physics with appropriate effective transport and thermodynamic properties. This modeling approach requires the assumption of local thermal equilibrium between the particle and gas phases to be valid and the gas phase must have a relative velocity with respect to the particle phase of approximately zero.

In our previous work, a 2-D steady-state modeling approach for predicting overall heat transfer coefficients was developed (Albrecht & Ho, 2017) and a 1-D transient model was developed for the study of heat exchanger control (Fernandez-Torrijos et al., 2018). This work extends the prior studies by considering the flow configuration of $sCO_2$ and particles through reduced order modeling, which is predictive of overall heat transfer coefficients for thermally developing flow and appropriately captures the combined counter/cross-flow configuration. The model allows for rapid solutions and parametric studies of heat exchanger design and sensitivity analysis. The methodology also provides the basis for future studies on design consideration for thermo-mechanical stress and technoeconomic analysis for minimizing heat exchanger cost.

### 4.1. Reduced order heat exchanger model

The following section details the reduced order modeling approach and solution methodology that has been developed in Engineering Equation Solver (F-Chart, 2017). Three regions are defined including the solid particle flow, heat transfer surface, and $sCO_2$ flow channels. The counter/cross-flow configuration of the overall heat exchanger (Fig. 1) is addressed using effectiveness-NTU relationships for each bank, and the inlet and outlet boundaries are linked in a way that provides a global counter-flow configuration. The modeling equations are developed for a single bank of parallel plates and the boundary conditions for linking multiple banks are given to represent the entire heat exchanger geometry.

The set of conservation equations that are solved for the system are given by Eqs. (2) and (3) where subscript s denotes the solid particle domain and subscript $CO_2$ denotes the $sCO_2$ domain.

$$\dot{Q}_{HX,i} = \dot{m}_s\left(h_s(T_{in,i}) - h_s(T_{out,i})\right) \tag{2}$$

$$\dot{Q}_{HX,i} = \dot{m}_{CO_2}\left(h_{CO_2}(T_{out,i}, P_{out,i}) - h_{CO_2}(T_{in,i}, P_{in,i})\right) \tag{3}$$

The two energy balances for the particle and $sCO_2$ domains within a given cross-flow plate bank are related through the ε-NTU relationship (Eqn. (4)) assuming both streams are unmixed.

$$\varepsilon_{HX,i} = 1 - \exp\left[\frac{NTU_i^{0.22}}{C_{R,i}}\left(\exp\left(-C_{R,i}NTU_i^{0.78}\right) - 1\right)\right] \tag{4}$$

To provide closure to the set of equations for a single plate bank, the capacitance ratio ($C_{R,i} = \dot{C}_{min,i}/\dot{C}_{max,i}$), number of transfer units ($NTU_i = U_iA_i/\dot{C}_{min,i}$), and heat exchanger effectiveness ($\varepsilon_{HX,i} = Q_{HX,i}/Q_{HX,max,i}$) must be determined based on the heat exchanger geometry and thermophysical properties of the heat transfer fluids. The capacitance of the particle and $sCO_2$ streams are based on the mass flow rate multiplied by the specific heat capacity, which is calculated at the average of the inlet and outlet temperatures of the bank. The overall heat transfer coefficient ($U_{HX,i}$) is determined based on a thermal resistance network using the $sCO_2$ channel convection coefficient ($\bar{h}_{CO_2}$), conduction through the heat exchanger material ($k_m$), near-wall particle thermal resistance ($R_c''$), and particle-wall convection coefficient ($\bar{h}_{sw}$). The overall heat transfer coefficient for a single bank can be calculated as

$$U_{HX,i} = \left(\frac{1}{\bar{h}_{CO_2}} + \frac{t_m}{k_m} + R_c'' + \frac{1}{\bar{h}_{sw}}\right)_i^{-1}. \tag{5}$$

The $sCO_2$ channel convection coefficient is calculated using the Gnielinski correlation (Gnielinski, 1976) with temperature averaged transport properties. The moving packed-bed heat transfer coefficient is calculated from the analytical solution for plug flow (Muzychka et al., 2010), which has been shown to be in agreement with experimentally measured values for circular (Watkins & Gould, 2017) and rectangular (Albrecht & Ho, 2018) channels. The moving packed-bed domain is modeled according to the single component continuum approximation. The particles are only considered to move in the vertical direction under the force of gravity. The Nusselt number ($\bar{Nu}_{Dh} = 2w_{ch}\bar{h}_{sw}/k_{s,eff}$) relationship (Eqs. (6) and (7)) (Muzychka et al., 2010) for parallel plates with a thermal entry is shown in Fig. 2, which can be used to calculate the average particle-wall convection coefficient from the heat exchanger geometric parameters and particle thermophysical properties.

$$\bar{Nu}_{Dh,H} = \left[\left(2\frac{0.886}{\sqrt{Gz^{-1}}}\right)^{12/5} + 12^{12/5}\right]^{5/12} \tag{6}$$

$$\bar{Nu}_{Dh,T} = \left[\left(2\frac{0.564}{\sqrt{Gz^{-1}}}\right)^{5/2} + 9.87^{5/2}\right]^{2/5} \tag{7}$$

The bulk effective thermal conductivity of the particle bed ($k_{s,eff}$) is the transport property that accounts for all modes of heat transport (interstitial gas conduction, particle-particle conduction, and particle surface radiation) through the bed of particles. The bulk effective thermal conductivity can be used with the Nusselt correlations to establish the solid-wall convection coefficient.

Within a bed of granular material, the solid volume fraction is lower at the heat transfer surface than within the bulk. Therefore, the bulk effective thermal conductivity of the packed bed based on bulk parameters is not representative of the behavior in the near-wall region. The near-wall void fraction ($\phi_{g,nw}$) can be calculated as

$$\phi_{g,nw} = (1 - \phi_g)(0.7293 + 0.5139Y) \tag{8}$$

where $\phi_g$ is the void fraction in the bulk and $Y$ is the ratio of the particle diameter to the curvature of the heat transfer surface (taken to be 0 for flat plates) (Botterill & Denloye, 1978). The near-wall void fraction can be used to calculate a new effective thermal conductivity that exists in the near-wall region. The first particle layer contact resistance with the heat transfer surface is accounted for with the contact resistance ($R_c''$) terms established in the thermal resistance network. Finally, the conduction through the heat exchanger material can be determined from the wall thickness and material thermal conductivity.

In order to solve the model for a series of plate banks where the $sCO_2$ and particles are globally in counter-flow configuration, boundary conditions as well as relationships for linking the plate banks must be established. The boundary conditions for the global particle and $sCO_2$ inlets are given by Eqn. (9) and (10), respectively. The coupling between banks of plates in series for the particle and $sCO_2$ streams is given by Eqn. (11) and (12), respectively.

$$T_{s,in,1} = T_{s,in} \tag{9}$$

$$T_{CO_2,in,N_{bank}} = T_{CO_2,in} \tag{10}$$

$$T_{s,in,i} = T_{s,out,i-1} \tag{11}$$

$$T_{CO_2,in,i-1} = T_{CO_2,out,i} \tag{12}$$

Eqs. (9) and (10) assume that the $sCO_2$ and particle flows exiting the individual banks are perfectly mixed prior to entering the next bank. The assumption is completely valid for the $sCO_2$ flow as the fluid exiting each bank is collected in headers at a single point and mixed before being introduced into the next bank. For the particle side, a temperature distribution can exist between banks over the plate width. However, since the plate alignment between banks is offset (Fig. 1), similar to a staggered tube array, particles are mixed over the channel width.

Global heat exchanger performance can be characterized according to the log mean temperature difference ($\Delta T_{lm}$) and overall heat transfer coefficient ($U_{HX}$), which can be calculated from post processing the model solution.

$$\Delta T_{lm} = \frac{(T_{s,out} - T_{CO_2,in}) - (T_{s,in} - T_{CO_2,out})}{\ln\left(\frac{T_{s,out} - T_{CO_2,in}}{T_{s,in} - T_{CO_2,out}}\right)} \tag{13}$$

$$U_{HX} = \frac{\sum_i \dot{Q}_{HX,i}}{A_{HX}} \tag{14}$$

Finally, the $sCO_2$ pressure drop, considering only major losses for channel flow through the heat exchanger plates, can be estimated through summing the pressure drop in each cross-flow bank according to the correlation of Li et al. (2011). This metric does not consider the minor losses due to piping connections between plate banks, but can provide insight into the tradeoff in heat transfer and pressure drop due to $sCO_2$ channel dimensions.

### 4.2. Particle thermophysical properties

Packed bed thermal conductivity of granular material has been studied through experimentation. However, knowledge of thermal conductivity of CSP relevant particle compositions at temperature (550–800 °C) are not well known. Bauman and Zunft have measured packed bed thermal conductivity of particle beds using an experiment designed for measuring the thermal conductivity of refractory material (Baumann & Zunft, 2015b) and found that the effective thermal conductivity increases significantly with temperature and particle diameter. For bauxite particles with a diameter of 600 μm, packed bed thermal conductivity was found to increase from 0.22 to 0.54 $W m^{-1} K^{-1}$ when increasing the temperature from ambient to 800 °C. The increased conductivity was attributed to increased thermal radiation at elevated temperature. Relevant particle compositions and sizes were also studied by Godbee and Ziegler (Godbee & Ziegler, 1966) who found similar dependencies of packed bed thermal conductivity on temperature and identified solid volume fraction as another important parameter.

To capture the effects of temperature and particle thermophysical properties on the bulk effective thermal conductivity of the moving packed bed of particles, the ZBS correlation (van Antwerpen et al., 2010) is implemented. The correlation requires knowledge of particle diameter, thermal conductivity, solid volume fraction, and interstitial gas transport properties. The dependence of the predicted bulk effective thermal conductivity on particle diameter and temperature is given in Fig. 3 for the particle properties given in Table 1.

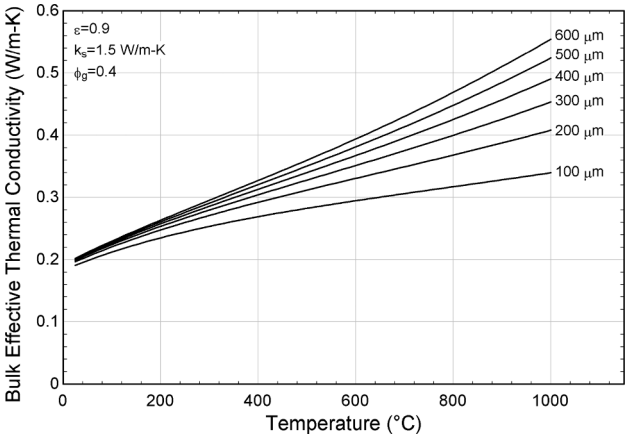


**Fig. 3.** Bulk effective thermal conductivity ($k_{s,eff}$) prediction of the ZBS correlation as a function of particle diameter and temperature.

**Table 1**
Particle thermophysical properties required by the ZBS correlation for predicting effective packed-bed thermal conductivity of sintered bauxite particles.

| Parameter | Value | Units | Ref. |
|---|---|---|---|
| Particle Diameter ($d_p$) | 100–600 | μm | |
| Particle Emissivity ($\varepsilon_s$) | 0.9 | – | Siegel et al. (2015) |
| Empirical Particle Contact ($\phi$) | 0.01 | – | van Antwerpen et al. (2010) |
| Particle Thermal Conductivity ($k_s$) | 2.0 | $W m^{-1} K^{-1}$ | |
| Gas Volume Fraction ($\phi_g$) | 0.45 | – | Ho et al. (2018) |
| Gas Thermal Conductivity ($k_g$) | Air (T) | $W m^{-1} K^{-1}$ | F-Chart (2017) |

The trends observed in experimental data are reflected in the predictions of the ZBS correlation. The packed-bed thermal conductivity is improved with larger particle diameters and elevated temperatures, but there are additional considerations when designing a heat exchanger and selecting particles for operation such as the near-wall thermal resistance, which will decrease heat transfer with increasing particle diameter, as well as channel width and particle flow consistency. Therefore, a tradeoff exists between heat exchanger geometry and particle thermophysical properties for maximizing heat exchanger conductance.

The contributing heat transfer mechanisms within the lumped bulk effective thermal conductivity term can be established from the ZBS correlation to determine the reason for temperature and particle diameter dependence. The three contributing heat transfer mechanisms for two particle diameters are plotted in Fig. 4. The value of the red line represents the contribution of particle surface radiation. The distance from the red line to the blue line represents the heat transport from particle to particle that occurs through the gas phase. Finally, the distance between the blue and black lines represents the contribution from particle-particle contact.

The effect of temperature on bulk effective thermal conductivity can be attributed to both the contribution through the interstitial gas as well as the surface radiation. Particle diameter can be observed to significantly increase the contribution from surface radiation at elevated temperatures. Since surface radiation makes a relatively small contribution to bulk effective thermal conductivity at low temperature, the effect of particle diameter is only observed at elevated temperature. The contribution of surface radiation to the bulk effective thermal conductivity increases with particle diameter since the emission from one particle to its adjacent particle moves a larger distance. In other

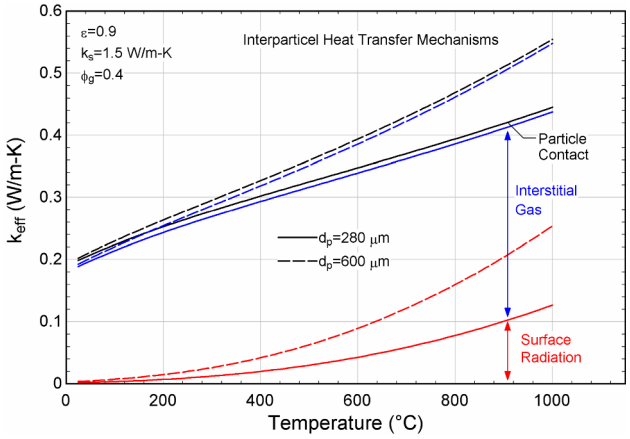


**Fig. 4.** Heat transfer mechanisms contributing to the bulk effective thermal conductivity ($k_{s,eff}$) of granular material as a function of temperature for two particle diameters.

words, each particle appears as a radiation shield where using larger particle diameters allows for fewer shields within a given channel dimension. However, to fully understand the effect of particle diameter on heat exchanger performance a parametric study of particle diameter must be conducted.

Thermodynamic properties of bauxite particles are well known (Siegel et al., 2015) and have been measured experimentally and found to have a temperature-dependent heat capacity. The particle specific heat capacity, volume fraction, and density are independent of particle diameter and are given in Table 2.

### 4.3. Properties of $sCO_2$ and heat transfer material

Closure to the modeling equations is provided by the thermodynamic and transport properties of the $sCO_2$ working fluid and heat exchanger material. The $sCO_2$ thermophysical properties are taken from the work of Span et al. (Span & Wagner, 1996) and Vesovic et al. (1990) for the thermodynamic and transport properties, respectively. The temperature dependent properties of SS316 are taken from EES material thermophysical property database based on the work of Ho & Chu (1977).

### 4.4. Heat exchanger boundary conditions

The boundary conditions for the particle/$sCO_2$ heat exchanger are selected based on the use of the recompression closed Brayton cycle (RCBC) (Ho et al., 2016a, Ho et al., 2016b). The targeted $sCO_2$ turbine inlet (heat exchanger outlet) temperature is 700 °C for achieving a thermal efficiency of 50%. The heat exchanger $sCO_2$ inlet temperature is 550 °C, based on the temperature leaving the high-temperature recuperator of the RCBC cycle. The particle temperatures are selected to achieve a > 200 °C temperature difference from inlet to outlet for enabling thermal energy storage. Therefore, the particle inlet temperature is taken to be 775 °C and the particle outlet temperature is 570 °C. The choice of all four temperature boundary conditions results in heat exchanger log mean temperature difference ($\Delta T_{lm}$) of 41.61 °C. The sensitivity of the particle operating temperatures to the heat exchanger cost requirements for achieving the DOE cost metric of \$150 $kW_t^{-1}$ will be addressed in a future section.

## 5. Discussion

### 5.1. Heat transfer performance of baseline geometry

The baseline geometry for a shell-and-plate moving packed-bed particle-to-$sCO_2$ heat exchanger is considered to have the parameters given in Table 3, which are based on the prototype heat exchanger geometry presented by Ho et al. (2018).

Simulating the baseline geometry with the reduced order methodology described above results in an overall heat transfer coefficient of 244 $W\,m^{-2}K^{-1}$ and a pressure drop of 55.7 kPa in the $sCO_2$ stream. For this configuration, particle velocities will be approximately 6.6 $mm\,s^{-1}$ resulting in an inverse Gratez number of 0.037, which will produce a slight improvement in the particle-wall heat transfer due to the flow being in the thermally developing regime. The $sCO_2$ convection coefficient is found to be 2440 $W\,m^{-2}K^{-1}$ and the effective particle side heat transfer coefficient (bulk convection and near-wall thermal resistance) is found to be 313 $W\,m^{-2}K^{-1}$ with slight variations between banks due to the temperature variations. Therefore, approximately 12% of the thermal resistance can be attributed to the $sCO_2$ convection and 87% can be attributed to the particle heat transfer resistance. The particle side thermal resistance can be further divided into 73% being attributed to the bulk convection and 14% to the near-wall thermal resistance.

From the analysis of the baseline geometry, it is possible to consider the potential heat transfer performance improvements and engineering tradeoffs that occur through modifying the geometry. The geometry can be altered through changing the heat exchanger plate dimensions, number of plate banks, heat exchanger plate spacing, and $sCO_2$ channel geometry. As will be discussed in a future section, the choice of particle diameter is also closely tied to the choice of heat exchanger geometry. Thus, it is important to consider particle thermophysical properties while assessing changes in the heat exchanger geometry to improve heat transfer performance. The following sections are dedicated to parametric and sensitivity analysis on the design and operating conditions of the heat exchanger geometry discussed above.

### 5.2. Plate geometry and $sCO_2$ channel dimensions

The geometry of the heat exchanger plates can have a large influence on the overall heat transfer coefficient as well as the pressure drop experienced in the $sCO_2$ channels. The design parameters include the plate width and height as well as the $sCO_2$ channel dimensions. In this study, the surface area of the individual heat exchanger plates has been fixed at 0.1 $m^2$ and held constant between the banks for simplicity. The plate geometry is adjusted though changing the aspect ratio ($H/L$), which is defined here as the plate height (particle flow direction) divided by the plate width ($sCO_2$ flow direction).

The tradeoff between these geometric design parameters is illustrated in Fig. 5. Conditions that improve the overall heat transfer coefficient are observed to increase the $sCO_2$ pressure drop. For the $sCO_2$ channel geometry, reduction in the diameter of channels within the plates results in shorter diffusion lengths for heat transfer (i.e., improved $sCO_2$ convection coefficients $\bar{h}_{CO_2}$), which improves overall heat transfer coefficients. However, the pressure drop is significantly increased through reducing channel diameter. Since the majority of the thermal resistance in the baseline geometry has been attributed to the particle side, changes in the $sCO_2$ channel geometry are not shown to have a large impact on the overall heat transfer coefficient.

The aspect ratio of the heat exchanger plates can have a similar effect on the overall heat transfer coefficient and $sCO_2$ pressure drop.

**Table 2**
Particle thermophysical properties independent of particle diameter for modeling sintered bauxite particles.

| Parameter | Value | Units |
|---|---|---|
| Density ($\rho_s$) | 3300 | $kg\,m^{-3}$ |
| Volume Fraction ($\phi_s$) | 0.55 | – |
| Specific Heat Capacity ($c_{p,s}$) | $148.2T_s^{0.3093}$ | $J\,kg^{-1}K^{-1}$ |

**Table 3**
Baseline heat exchanger geometric design parameters based on the heat exchanger geometry presented by (Ho et al., 2018).

| Parameter | Value | Units |
|---|---|---|
| Number of banks | 4 | – |
| Plate surface area | 0.1 | $m^2$ |
| Plate aspect ratio | 0.5 | – |
| $sCO_2$ channel diameter | 1.0 | mm |
| $sCO_2$ channel spacing | 1.0 | mm |
| Material thickness | 1.0 | mm |
| Particle diameter | 280 | μm |
| Particle channel width | 6.0 | mm |

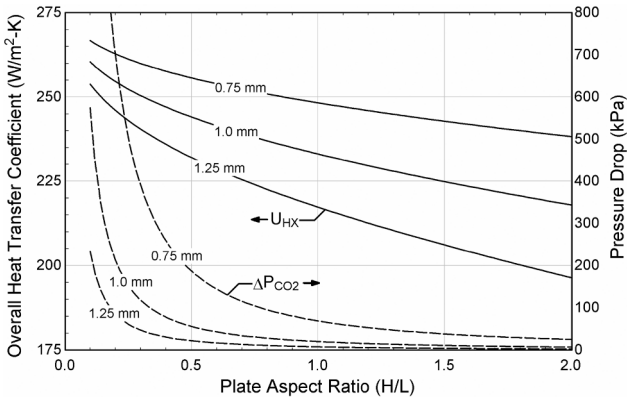


**Fig. 5.** Overall heat transfer coefficient and pressure drop as a function of heat exchanger plate geometry and $sCO_2$ channel diameter.

Higher aspect ratios result in reduced flow length for the $sCO_2$ stream as well as larger cross-sectional area for the flow. Therefore, the $sCO_2$ pressure drop is reduced due to a reduced channel velocity as well as flow length. However, the overall heat transfer coefficient is reduced since the $sCO_2$ channel Nusselt correlation is dependent on the Reynolds number of the flow. The change in the plate geometry does not have a significant impact on the particle-wall heat transfer coefficient because the correlations (Fig. 2) are not dependent on the Reynolds number of the particle flow and the inverse Graetz number remains constant with corresponding increases in particle flow length and velocity.

### 5.3. Considerations for approaching the counter-flow limit

Constructing a heat exchanger from multiple cross-flow units arranged in a counter-flow configuration approximates the performance of a counter-flow device. In addition, the spacing in between each bank provides a cross-channel mixing region where the thermal boundary layer developed in the particle flow is disrupted and the heat transfer coefficient in the following bank is enhanced due to a thermal entry. To address the design considerations for selecting the number of banks in a heat exchanger, simulations with an increased number of cross-flow banks in a counter-flow configuration were conducted.

The effect of increasing the number of banks on the overall heat transfer coefficient and $sCO_2$ pressure drop for fixed temperature boundary conditions and plate geometry is given in Fig. 6. The simulations begin at three plate banks because fewer banks are unable to achieve the required heat exchanger effectiveness to meet the specified $sCO_2$ and particle outlet temperature. Increasing the number of plate banks displays an improvement in the overall heat transfer coefficient with diminishing return. The improvement in overall heat transfer coefficient is the result of the device approaching the counter-flow limit as well as increasing the number of thermal entries (i.e., improved particle cross-channel mixing). However, the $sCO_2$ pressure drop is shown to increase with increasing number of plate banks. As the number of plate banks is increased, the length of the $sCO_2$ flow path is increased as well as the $sCO_2$ channel velocity. Therefore, $sCO_2$ pressure drop is shown to have an exponential relationship with the number of plate banks.

A more representative comparison would be to fix the $sCO_2$ pressure drop though adjusting the $sCO_2$ channel dimension and study the influence of increasing the number of heat exchanger banks. The results are depicted in Fig. 7 considering a heat exchanger constructed of three to ten banks. Significant increases (~10%) in the overall heat transfer coefficient are possible if the allowable pressure drop of the device is increased from 50 to 400 kPa. The increase in the overall heat transfer coefficient is observed to be more significant at higher numbers of plate banks due the heat transfer becoming more limited by the $sCO_2$ convection coefficient in that regime. However, an increase in the pressure drop across the primary heat exchanger will result in a decreased $sCO_2$ cycle efficiency, which must be considered within technoeconomic studies to establish the optimal operating conditions.

### 5.4. Considerations for particle diameter and plate spacing

Particle diameter and plate spacing are two of the most important terms in the design and operation of the heat exchanger that influence the overall heat transfer coefficient. Since the majority of the thermal resistance for particle-to-$sCO_2$ heat transfer is due to the thermal conductivity of the packed bed, reducing the diffusion length (channel width) for heat transfer or improving the thermal conductivity of the packed bed ($k_{s,eff}$) will directly improve the overall heat transfer coefficient. However, there are limitations associated with the particle diameters that are allowable within a given channel geometry. Channel width must be 10 particle diameters or greater to achieve uniform and consistent flow of particles between parallel plates. Therefore, a tradeoff exists between increasing the thermal conductivity through using larger particle diameters and the use of narrow channels which require smaller particle diameters.

The modeling results for the nominal heat exchanger configuration with variations in particle diameter and channel width are displayed in Fig. 8. The plotted lines indicate the dependence of overall heat transfer coefficient on particle diameter for fixed channel widths ($w_{ch}$). The dashed line indicates the limit for particle diameter that can be used with a given channel width. Improvements in overall heat transfer coefficient are observed for increasing particle diameters especially with larger channel widths. However, the most significant improvements for increasing particle diameter are observed to occur at particle diameters below 200 μm. At particle diameters above 150 μm, the relationship between overall heat transfer coefficient and particle diameter begins to asymptote to a constant value. This result is due to a tradeoff in increasing bulk effective thermal conductivity of the packed

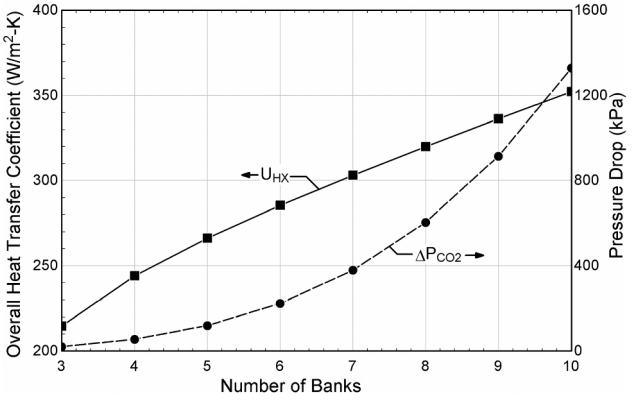


**Fig. 6.** Overall heat transfer coefficient and pressure drop with increasing number of cross-flow plate banks arranged in a counter-flow configuration.

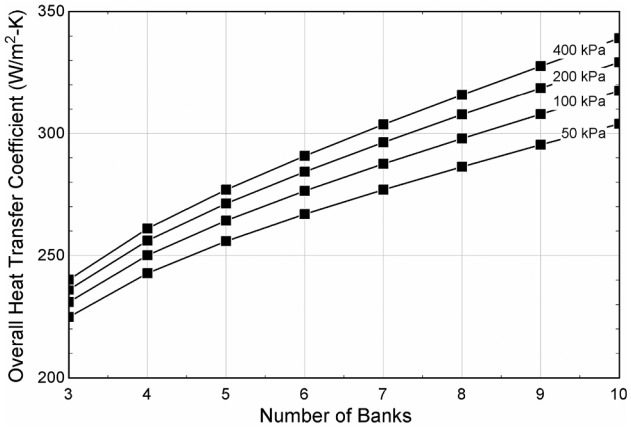


**Fig. 7.** Overall heat transfer coefficient at constant pressure drop with increasing number for cross-flow plate banks arranged in a counter-flow configuration.

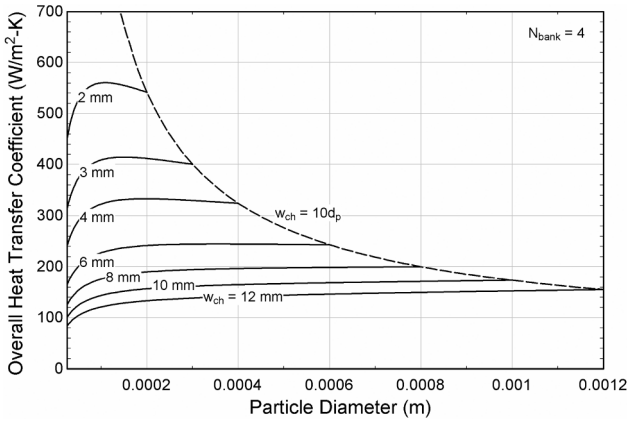


**Fig. 8.** Overall heat transfer coefficient as a function of particle channel width and particle diameter with the nominal plate geometry and number of banks.

bed and increasing the near-wall thermal resistance between the first particle layer and heat transfer surface. In fact, for small channel widths, the overall heat transfer coefficient displays an optimal particle size where further increases in particle diameter result in a reduction in overall heat transfer coefficient.

The overall heat transfer coefficient is observed to have a much stronger dependence on channel width. Reducing the channel width by a factor of two is observed to almost double the overall heat transfer coefficient. However, reductions in channel width lead to significant limitations on the allowable particle size range. For particle diameters in the 200–300 μm range, a channel width of 3–4 mm should be targeted. Future heat exchanger designs utilizing sintered bauxite particles should prioritize plate spacing as a means of improving overall heat transfer coefficient.

Since previous sections addressed $sCO_2$ pressure drop and increased number of plate banks as potential methods for improving overall heat transfer coefficient, the effect on overall heat transfer coefficient due to particle diameter and plate spacing should be investigated for constant $sCO_2$ pressure drop and an increased number of plate banks. The modeling results are displayed in Fig. 9 for a six-bank heat exchanger with a fixed pressure drop of 200 kPa. Marginal improvements in overall heat transfer coefficient are observed for small particle diameters in which the thermal resistance is dominated by the bulk effective thermal conductivity. Increasing the number of heat exchanger banks promotes cross channel mixing which improves heat transfer in the case of limited bulk effective thermal conductivity. However, significant improvements are observed for the small channel geometries and particle sizes when fixing $sCO_2$ pressure drop because the heat transfer is more limited by $sCO_2$ convection coefficient. Increasing the number of plate banks and fixing the $sCO_2$ pressure drop is shown to shift the optimal particle diameter for narrow channel geometries to a slightly smaller size. A channel geometry of 4 mm with a particle diameter of 200 μm can achieve an overall heat transfer coefficient approaching 400 $W\,m^{-2}\,K^{-1}$. The heat exchanger geometry is summarized in Table 4.

### 5.5. Sensitivity to particle thermophysical properties

The previous sections were all directed at the parameters for sintered bauxite particles while using the ZBS correlations to predict bulk effective thermal conductivity while determining the tradeoffs in performance due to heat exchanger geometry. Through performing a sensitivity analysis to particle parameters, the key limitations of sintered bauxite particles can be identified and targeted for improvement. The parameters to be varied are the particle emissivity, thermal conductivity of the bulk material, void fraction, and particle contact conduction term. The sensitivity of the overall heat transfer coefficient to possible variations in particle parameters for the nominal heat exchanger geometry are given in Table 5 as well as a heat exchanger with an improved geometry targeting an overall heat transfer coefficient of ~400 $W\,m^{-2}\,K^{-1}$.

The overall heat transfer coefficient is shown to be most dependent on the thermal conductivity of the base particle material and gas volume fraction of the packed bed. Therefore, altering the particle base material from the typical sintered bauxite could prove beneficial to a moving packed-bed heat exchanger. Additional improvements are possible through decreasing the gas volume fraction, which could be implemented through mixing particles of multiple diameter. However, it should be noted that the ZBS correlation was developed for packed beds of mono-sized spheres and effective thermal conductivity of packed beds with large size distributions requires further investigation.

Small improvements in overall heat transfer coefficient are possible through increased particle emissivity and enhanced particle-particle contact. However, these were shown to be relatively small contributions to the overall heat transfer coefficient. For small particle diameters it was shown that the contribution of heat transfer due to particle surface radiation decreases. Furthermore, particle-particle contact was shown to make a negligible contribution to the bulk effective thermal conductivity in the ZBS correlation.

### 5.6. Operating and cost considerations for application to particle-based CSP

Primary power cycle heat exchangers for next generation CSP

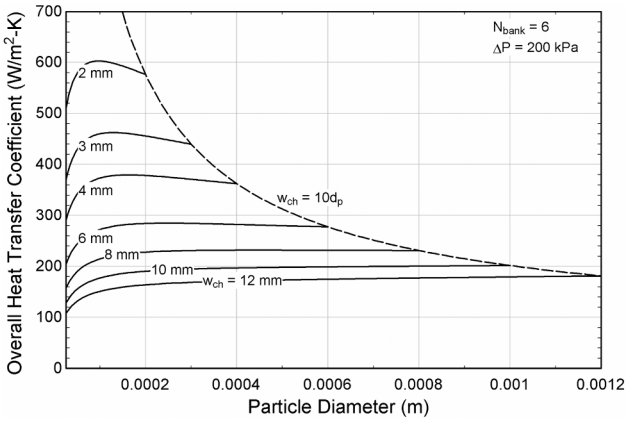


**Fig. 9.** Overall heat transfer coefficient as a function of particle channel width and particle diameter with fixed $sCO_2$ pressure drop and six heat exchanger banks.

**Table 4**
Improved heat exchanger geometry to approach an overall heat transfer coefficient of 400 $W\,m^{-2}\,K^{-1}$ with a pressure drop of 200 kPa.

| Parameter | Value | Units |
|---|---|---|
| Number of banks | 6 | – |
| Plate surface area | 0.1 | $m^2$ |
| Plate aspect ratio | 0.5 | – |
| $sCO_2$ channel diameter | 1.2 | mm |
| $sCO_2$ channel spacing | 1.0 | mm |
| Material thickness | 1.0 | mm |
| Particle diameter | 200 | μm |
| Particle channel width | 4.0 | mm |

systems have been targeted to be < \$150 $kW_t^{-1}$ to meet the DOE's 2020 cost target of \$0.06 $kW^{-1}hr^{-1}$ LCOE (Mehos et al., 2016). In addition, a potential path to achieving 2030 cost targets of \$0.05 $kW^{-1}hr^{-1}$ LCOE is a reduction in heat exchanger cost to < \$100 $kW_t^{-1}$ (Vijaykumar et al., 2018). Based on the cost metrics and heat exchanger model developed above, cost targets per $m^2$ of heat transfer area can be established for the shell-and-plate moving packed-bed heat exchanger. The relationship between the cost per surface area ($C_A$), overall heat transfer coefficient ($U_{HX}$), log mean temperature difference ($\Delta T_{lm}$), and cost target per $kW_t$ ($C_P$) can be expressed as

$$C_A = C_P U_{HX} \Delta T_{lm}, \quad (15)$$

which allows for the tradeoffs in operating conditions and allowable costs to be observed.

The dependence of the allowable cost of the heat transfer surface area is depicted in Fig. 10. The simulations were conducted by fixing the particle outlet temperature and adjusting the log mean temperature difference by increasing the particle inlet temperature. Therefore, larger log mean temperature difference also results in increased temperature difference between the hot and cold storage bins for sensible energy storage. Higher values of log mean temperature difference are shown to be able to tolerate higher heat transfer surface area costs because less surface area is required if the temperature driving force is increased. Furthermore, reduction in the cost target per $kW_t$ is shown to significantly limit the allowable cost per heat transfer area. To achieve DOE's 2020 cost targets (\$150 $kW_t^{-1}$) heat transfer surface area must be produced at approximately \$2400 $m^{-2}$ considering the nominal particle temperature conditions ($\Delta T_{lm} = 41.61$ °C) and the heat exchanger geometry in Table 4. If the log mean temperature difference is allowed to increase to a value of 50 °C, the allowable cost of the heat transfer surface area can be increased to \$2950 $m^{-2}$ while still meeting the cost target of \$150 $kW_t^{-1}$. However, this increase will result in a reduction in the solar thermal efficiency of the receiver, but decrease the mass of particles and volume of the storage bins required by the thermal energy storage subsystem. The selection of these operating conditions and their impact on the overall economics of a particle-based CSP system needs to be addressed in future technoeconomic studies where the cost of additional high-temperature material and reduction in the solar thermal receiver efficiency are considered when increasing the primary power cycle heat exchanger log mean temperature difference.

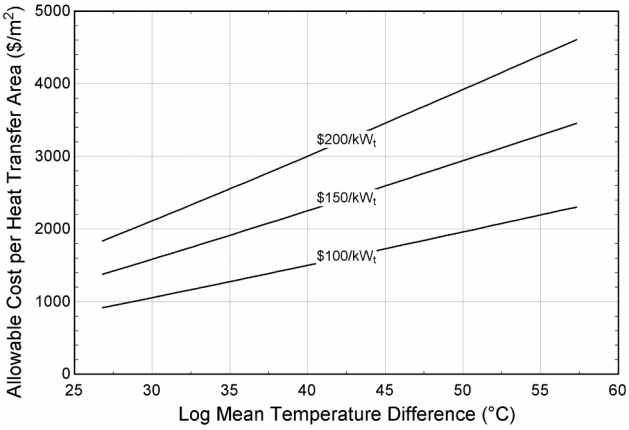


**Fig. 10.** Allowable cost of heat transfer surface area as a function of heat exchanger cost targets and operating conditions.

## 6. Conclusion

A modeling methodology for a shell-and-plate moving packed-bed heat exchanger was developed for the application of particle-to-$sCO_2$ heat transfer for next-generation CSP plants. The reduced order modeling methodology is robust and captures the relevant physics for dense granular flow heat transfer, but is lightweight enough to be exercised in parametric studies to guide the development and design of moving packed-bed heat exchangers. The importance of a coupled selection of particle size and channel geometry was established where tradeoffs in near-wall thermal resistance and thermal conductivity of the packed bed were observed. Future designs should prioritize the development of heat exchangers with reduced channel dimensions and increased number of plate banks to improve heat transfer. In addition, optimal particle size was identified, which was shown to be specific to the heat exchanger geometry. For a channel width of 4 mm, the overall heat transfer coefficient of the heat exchanger is optimized with approximately 175 μm. Overall heat transfer coefficients approaching 400 $W\,m^{-2}\,K^{-1}$ are possible for particle channel widths of 4 mm with 200 μm. Furthermore, the effect of improvements in particle thermophysical properties on overall heat transfer coefficient identified particle thermal conductivity and packed bed void fraction as important parameters that can lead to improvements of 27 and 52 $W\,m^{-2}\,K^{-1}$, respectively. Finally heat exchanger cost was discussed relative to the 2020 SunShot target. To achieve primary heat exchanger costs < \$150 $kW_t^{-1}$, diffusion bonded plates must be produced at less than \$2400 $m^{-2}$.

**Table 5**
Sensitivity of overall heat transfer coefficient to particle thermophysical properties.

| | Parameter | Variation | $\Delta U_{HX}$ ($W\,m^{-2}\,K^{-1}$) |
|---|---|---|---|
| Baseline Geometry | Particle Emissivity ($\varepsilon_s$) | 0.9 ± 0.09 | ± 0.601 |
| | Particle Conductivity ($k_s$) | 2.0 ± 1.0 | ± 21.1 |
| | Empirical Particle Contact ($\phi$) | 0.01 ± 0.01 | ± 1.08 |
| | Gas Volume Fraction ($\phi_g$) | 0.45 ± 0.1 | ± 35.0 |
| Improved Geometry | Particle Emissivity ($\varepsilon_s$) | 0.9 ± 0.09 | ± 0.542 |
| | Particle Conductivity ($k_s$) | 2.0 ± 1.0 | ± 27.3 |
| | Empirical Particle Contact ($\phi$) | 0.01 ± 0.01 | ± 1.81 |
| | Gas Volume Fraction ($\phi_g$) | 0.45 ± 0.1 | ± 52.5 |

## Acknowledgements

The paper is based upon work supported in part by the DOE Solar Energy Technologies Office (SuNLaMP-0000000-1507). Sandia National Laboratories is a multimission laboratory managed and operated by National Technology and Engineering Solutions of Sandia, LLC, a wholly owned subsidiary of Honeywell International Inc., for the U.S. Department of Energy's National Nuclear Security Administration under contract DE-NA0003525.

## References

Albrecht, K.J., Ho, C.K., 2017. Heat transfer models of moving packed-bed particle-to-$sCO_2$ heat exchangers. In: Proceedings of the ASME 2017 11th International Conference on Energy Sustainability, Charlotte.

Albrecht, K.J., Ho, C.K., 2018. High-temperatur flow testing and heat transfer for a moving packed-bed particle/sCO2 heat exchanger. AIP Conf. Proc. 2033 (1), 040003-1-9.

Alvia-Marin, A.L., 2011. Volumetric receivers in solar thermal power plants with central receiver system technology: a review. Sol. Energy 85 (5), 891–910.

Baumann, T., Zunft, S., 2012. Theoretical and experimental investigation of a Moving Bed Heat Exchanger for Solar Central Receiver Power Plants. In: 6th European thermal sciences conference, pp. 1–8.

Baumann, T., Zunft, S., 2015a. Development and performance assessment of a moving bed heat exchanger for solar central receiver power plants. Energy Procedia 69 (1), 748–757.

Baumann, T., Zunft, S., 2015b. Properties of granular materials as heat transfer and storage medium in CSP application. Solar Energy Mater. Solar Cells 143, 38–47.

Botterill, J.M., Denloye, A.O., 1978. A theoretical model of heat transfer to a packed or quiescent fluidized bed. Chem. Eng. Sci. 33 (4), 509–515.

Byman, A.D., Charles, T.L., Huang, X., 2014. Heat exchanger for cooling or heating bulk solids. United States, Patent No. US20140246184.

Carlson, M.D., Middleton, B.M., Ho, C.K., 2017. Techno-economic comparison of solar-driven $sCO_2$ brayton cycles using component cost models baselined with vendor data and estimates. In: Proceedings of the ASME 2017 Power and Energy Conference, Charlotte, North Carolina.

Chen, J.C., Grace, J.R., Golriz, M.R., 2005. Heat transfer in fluidized beds: design methods. Powder Technol. 150 (2), 123–132.

F-Chart, 2017. EES: Engineering Equation Solver. Middleton.

Fernandez-Torrijos, M., Albrecht, K.J., Ho, C.K., 2018. Dynamic modeling of a particle/sCO2 heat exchanger for transient analysis and control. Appl. Energy 226, 595–606.

Gnielinski, V., 1976. New equations for heat and mass transfer in turbulent pipe and channel flow. Int. Chem. Eng. 16, 359.

Godbee, H.W., Ziegler, W.T., 1966. Thermal Conductivities of MgO Al2O3 and ZrO2 Powders to 850C I. Experimental. J. Appl. Phys. 37 (1), 40–55.

Gomez-Garcia, F., Gauthier, D., Flamant, G., 2017. Design and performance of a multi-stages fluidised bed heat exchanger for particle-receiver solar power plants with storage. Appl. Energy 190, 510–523.

Henda, R., Falcioni, D.J., 2006. Modeling of heat transfer in a moving packed bed: case of the preheater in nickel carbonyl process. J. Appl. Mech. 73, 47–53.

Hiromi, T., 1996. Particles flow pattern and local heat transfer around tube in moving packed bed. AIChE J. 42 (6), 1621–1626.

Ho, C., 2016. A review of high-temperature particle receivers for concentrating solar power. Appl. Therm. Eng. 109 (1), 958–969.

Ho, C.K. et al., 2018. Evaluation of alternative designs for a high temperaure particle-to-$sCO_2$ heat excahnger. In: Proceedings of the ASME 2018 Power and Energy Conference, Lake Buena Vista, Florida.

Ho, C.K., Carlson, M., Garg, P., Kumar, P., 2016a. Technoeconomic analysis of alternative solarized sCO2 brayton cycle configurations. J. Sol. Energy Eng. 138 pp. 051008-1.

Ho, C.K., et al., 2016b. On-sun testing of an advanced falling particle receiver system. In: AIP Conference Proceedings, 1734(030022), pp. 1–8.

Ho, C.Y., Chu, T.K., 1977. Electrical Resistivity and Thermal Conductivity of Nine Selected AISI Stainless Steels. CINDAS.

Li, P., Seem, J.E., Li, Y., 2011. A new explicit equation for accurate friction factor calculation of smooth pipes. Int. J. Refrig. 34 (6), 1535–1541.

Ma, Z., Martinek, J., 2017. Fluidized-bed heat transfer modeling for the development of particle/supercritical-$CO_2$ heat exchanger. In: Proceedings of the ASME 2017 Power and Energy Conference, Charlotte, North Carolina.

Ma, Z., Mehos, M., Glatzmaier, G., Sakadjian, B.B., 2015. Development of a concentrating solar power system using fluidized bed technology for thermal energy conversion and solid particles for thermal energy storage. Energy Procedia 69, 1349–1359.

Mehos, M., et al., 2016. On the Path to SunShot: Advancing Concentrating Solar Power Technology, Performance, and Dispatchability. National Renewable Energy Laboratory, Golden, CO.

Muzychka, Y.S., Walsh, E., Walsh, P., 2010. Simple models for laminar thermally developing slug flow in noncircular ducts and channels. J. Heat Transf. 132 (11) pp. 111702-1-10.

Niegsch, J., Koneke, D., Weinspach, P.-M., 1994. Heat transfer and flow of bulk solids in a moving bed. Chem. Eng. Process. 33, 73–89.

Obuskovic, N., 1985. Heat Transfer Between Moving Beds of Solids and a Transverse Finned Tube, Oregon State University: Masters Thesis.

Obuskovic, N., 1988. Heat Transfer Between Moving Beds of Solids and a Vertical Tube, Oregon State University: PhD Thesis.

Park, S.I., 1996. Performance analysis of a moving-bed heat excahnger in vertical pipes. Energy 21 (10), 911–918.

Siegel, N.P., Gross, M.D., Coury, R., 2015. The development of direct absorption and storage media for falling particle solar central receivers. J. Solar Energy Eng. 137.

Span, R., Wagner, W., 1996. A new equation of state for carbon dioxide covering the fluid region form the triple-point temperature to 1100 K at pressures up to 800 MPa. J. Phys. Chem. Ref. Data 25 (6), 1509–1596.

Stein, W.H., Buck, R., 2017. Advanced power cycles for concentrated solar power. Sol. Energy 152, 91–105.

Turchi, C.S., Ma, Z., Neises, T.W., Wagner, M.J., 2013. Thermodynamic study of advanced supercritical carbon dioxide power cycles for concentrating solar power systems. J. Sol. Energy Eng. 135 (4).

van Antwerpen, W., du Toit, C.G., Rousseau, P.G., 2010. A review of correlations to model the packing structure and effective thermal conductivity in packed beds of mono-sized spherical particles. Nucl. Eng. Des. 240 (7), 1803–1818.

Vesovic, V., et al., 1990. The transport properties of carbon dioxide. J. Phys. Chem. Ref. Data 19 (3), 763–808.

Vijaykumar, R., Bauer, M., Lausten, M., Shultz, A., 2018. Optimizing the spercritical $CO_2$ brayton cycle for concentrating solar power application. In: The 6th International Supercritical CO2 Power Cycles Symposium, Pittsburgh.

Watkins, M.F., Gould, R.D., 2017. Heat Transfer To Vertical Dense Granular Flows at High Operating Temperatures. Charlotte, s.n.

Zanganeh, G., et al., 2012. Packed-bed thermal storage for concentrated solar power – Pilot-scale demonstration and industrial-scale design. Sol. Energy 86 (10), 3084–3098.